Paper 179

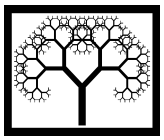

Proceedings of the Twelfth International Conference
on Computational Structures Technology,
B.H.V. Topping and P. Iványi, (Editors),
Civil-Comp Press, Stirlingshire, Scotland.

A Constitutive Three-Dimensional Interface Model for Masonry Walls subjected to High Strain Rates

P.B. Lourenço, S. Hashemi and J.M. Pereira
ISISE, Department of Civil Engineering
University of Minho
Guimarães, Portugal

Abstract

Investigation of the dynamic properties of construction materials is critical for structural engineering. The strain rate effect influences the properties of most constructions materials and this effect on materials such as concrete or steel has been intensively investigated. However, such studies on masonry materials are scarce. Understanding the strain rate effect on masonry materials is important for proper modelling and design of masonry structures under high velocity impacts or blast loads. The work, described in this paper, aims to study the behaviour of masonry at different strain rates. First, a drop weight impact machine is used at different heights and weights introducing different levels of strain rate. Then, a dynamic constitutive material interface model that includes an non-associated flow rule and high strain rate effects is proposed. The model capability is validated with numerical simulations of unreinforced block work masonry walls subjected to impact.

Keywords: masonry, drop weight, dynamic increase factor, interface model, out-of-plane behaviour.

1 Introduction

Different loading conditions might lead to different strain rates. Quasi-static loading produces strain rates of around 10^{-5} s^{-1}, while impacts and blast loading produce strain rates of well over 100 s^{-1}. When subjected to dynamic loading conditions, materials can have a much different behaviour when compared with their static behaviour [1]. Most research work on structural response and damage under impact and blast loading assumes typically static material properties, e.g. [2]. This can lead to an inaccurate prediction of structural damage and fragmentation.

Construction materials such as concrete or reinforcement bars have been studied under strain rate effects, which is a phenomenon already introduced into some standards. However, very limited studies can be found in the literature on masonry

materials, such as clay bricks or mortar, and the few authors use rather different equipment. Recently, Hao and Tarasov [3] conducted an experimental study under dynamic uniaxial compression using a Triaxial Static-Dynamic Testing Machine. Burnett *et al.* [4] presented also results from dynamic tensile experiments on a mortar joint using a specially designed Split-Hopkinson pressure bar. Asprone *et al.* [5] studied this effect on a specific Italian stone using a Hydro-Pneumatic Machine and a modified Hopkinson bar for tensile tests. Here, an experimental campaign on the influence of the strain rate on the mechanical properties of masonry and its components is described first. The tests were conducted with a Drop Weight (DW), which consists of a "hammer" with a given mass being released at a chosen height.

A series of experimental studies in masonry panels and structures has also been carried out to report their blast response, including maximum deflection and failure mechanisms of collapse, and to evaluate their performance. Varma et *al.* [6] provided the maximum deflection, the damage level, the reflected pressure, and the reflected impulse of 27 full scale tests with different thickness on brick panels subjected to blast loading. Evaluation of structural masonry damage and fragmentation of non-retrofitted masonry walls has also been of interest in a number of studies, e.g. [7]. The crack patterns of unreinforced masonry walls were classified into two groups based on the time of formation in [8]. These walls were subjected to low velocity impacts.

Due to the costs of laboratory tests, it is impossible to carry out a large number of tests. This would allow obtaining a comprehensive field test database, including most likely responses. Currently, given the development of computer technology, it is easy to have more detailed and accurate predictions, including dynamic response and localized damage through numerical simulations. Two common strategies have been developed for numerical simulation of masonry in the literature, namely micro strategy and macro strategy [9]. Within, the macro approach, homogenization techniques incorporate the geometry at micro-level and became rather popular in the last decades [10]. Depending upon the required accuracy, reliability, availability and computational costs, one of the approaches can be selected.

In present paper, a newly developed dynamic interface model accounting for strain rate effects is proposed for numerical simulations of the structural response of masonry walls subjected to impact using the finite element (FE) code ABAQUS. The rate-dependent failure envelop is divided into three parts, namely tension mode, coulomb friction mode, and compressive cap mode on the basis of the corresponding failure mechanisms. A comparison between numerical results and field test data obtained in [8] is performed to evaluate the performance of the proposed material model and the accuracy of the simulation in predicting the impact response and damage of masonry walls.

2 Mechanical Characterization

A Drop Weight Impact Machine (DW) was used to perform compression tests at different strain rates, see Figure 1. The load profile was measured at the base of the test specimen using a load cell specifically for dynamic applications. The deformation behaviour of the specimen was made using a FastCam video camera,

with a maximum frame rate of 250 000 frames per second. This strain measurement was possible using targets in the specimen at a specific location and performing a tracking sweep of those targets in the videos, for cost-efficiency reasons. The methodology was assessed with strain gauges, placed in each face of the specimen for a small number of specimens tested dynamically. In the quasi-static tests used as reference, strain gauges were also used to measure the strains in the specimen.

2.1 Adopted Materials

Handmade solid bricks were used to replicate old bricks. The bricks measured 20x10x5 cm in dimensions and from each brick, five specimens were prepared, with 7x3x3 cm. A commercial ready-mix mortar was used, with the same dimensions for the specimens. The masonry specimens were composed of four clay bricks and three mortar joints with one centimetre thickness, arranged in a stacked pattern. Test setup limitations lead to the final dimensions of 23x8x8 cm for the masonry specimens.

Figure 1: Drop Weight tower.

2.2 Mechanical Properties

In order to have the quasi-static reference for comparison with the results subjected to the dynamic regime, an experimental campaign on the behaviour under quasi-static uniaxial compression was performed. The mechanical properties under study were: a) compressive strength (σ_{max}); b) strain at peak strength (ε_u); c) Young's

modulus (E); and d) compressive fracture energy (G_c). Figure 2 shows the typical stress-strain relation and stress-displacement relation with information on how to determine these mechanical properties. A total of 5 (five) specimens of handmade clay brick, 9 (nine) specimens of mortar and 4 (four) specimens of masonry were tested. The brick specimens have the highest compressive strength with 13.59 MPa, whereas the mortar has strength of 4.46 MPa. This resulted in masonry specimens with 7.94 MPa of compressive strength. Also important, the Young's modulus is 2.32 GPa for the brick specimens and 0.80 GPa for the masonry specimens. The fracture energy in compression is similar for brick and mortar specimens, with 1.56 N/mm and 1.43 N/mm respectively, while for masonry the fracture energy is much larger, reaching 7.64 N/mm. The reason for this is that the masonry specimens showed higher deformation capacity due to the interaction between the masonry components.

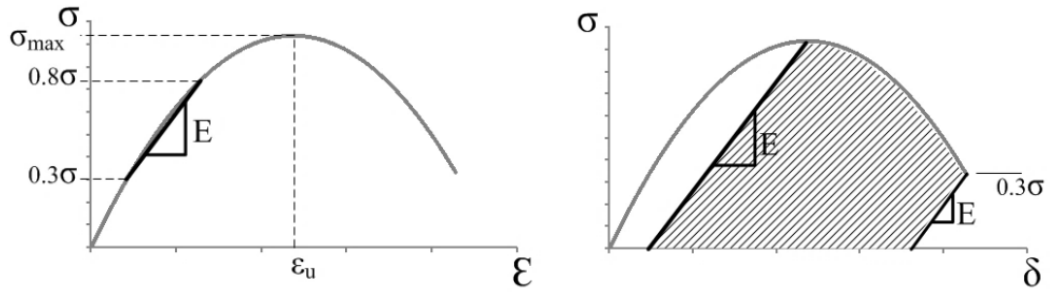

a) b)

Figure 2: Typical relations and obtained mechanical properties: a) stress – strain; b) stress – displacement.

For the dynamic regime testing, the Drop Weight (DW) impact machine was used. Several impact tests under uniaxial compression were performed. As stated previously, the objective is to obtain the stress-strain relations from the data recorded at the load cell acquisition and the fastcam video. To facilitate the treatment of the data obtained, the stress-time curve was approximated to a second degree polynomial, while the strain-time curve was approximated to a linear function. As a result, the final shape of the stress-strain curves is a second degree polynomial and can be seen in Figure 3 for the brick specimens.

With the stress-strain relations for each test, the m echanical properties could be determined and the dynamic increase factor (DIF) could be calculated as a function of the strain rate, according to the following equation:

$$DIF = \frac{Property\ (Dynamic)}{Property\ (Static)}, f(\dot{\varepsilon}) \tag{1}$$

These results were used to establish the relations between the mechanical properties and the strain rate. These relations are described as bi-log-linear relations, meaning that they can be written with two log-linear functions, low slope for the quasi-static regime and high slope for the dynamic regime. In order to simplify these relations,

the first log-linear function for the quasi-static regime was considered constant and set as DIF equals to 1 (one) until the point where the regime changes to dynamic.

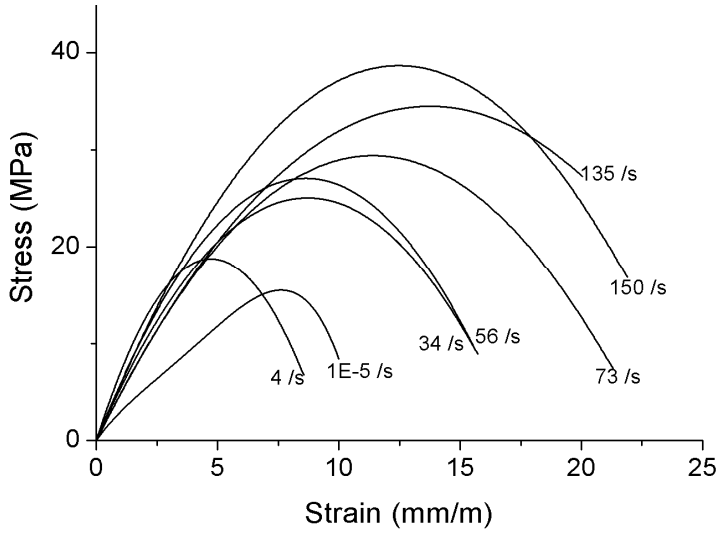

Figure 3: Examples of stress-strain curves at different strain rates (for clay brick).

A total of 58, 54 and 12 specimens of clay brick, mortar and masonry, respectively, were successfully tested under uniaxial compression, with strain rate ranging from 4 s^{-1} to 199 s^{-1}. Figure 4 shows typical examples of the relation between the dynamic increase factor and the strain rate for the compressive strength, for the clay brick. As expected the strain rate influences the compressive strength of this material and the dynamic increase factor for a strain rate of 200 s^{-1} is 2.5, meaning that the compressive strength is two and a half times the static value at that strain rate. The log-linear trend-line has a coefficient of determination R^2 higher than 70%, which for this material was considered good. The best-fitted equations of DIF as a function of strain rate were the following, full details can be found in [11]:

$$DIF(\sigma_u) = \begin{cases} 1 & if \quad 1E-5s^{-1} < \dot{\varepsilon} < 2s^{-1} \\ 0,3344\ln(\dot{\varepsilon}) + 0.7682 & if \quad 2s^{-1} < \dot{\varepsilon} < 200s^{-1} \end{cases} \tag{2}$$

$$DIF(E) = \begin{cases} 1 & if \quad 1E-5s^{-1} < \dot{\varepsilon} < 2s^{-1} \\ 0,3105\ln(\dot{\varepsilon}) + 0.7848 & if \quad 2s^{-1} < \dot{\varepsilon} < 200s^{-1} \end{cases} \tag{3}$$

$$DIF(\varepsilon_u) = \begin{cases} 1 & if \quad 1E-5s^{-1} < \dot{\varepsilon} < 2s^{-1} \\ 0,0673\ln(\dot{\varepsilon}) + 0.9533 & if \quad 2s^{-1} < \dot{\varepsilon} < 200s^{-1} \end{cases} \tag{4}$$

$$DIF(\mathrm{G}_C) = \begin{cases} 1 & if \quad 1E-5s^{-1} < \dot{\varepsilon} < 5s^{-1} \\ 1,3419\ln(\dot{\varepsilon}) - 1.1597 & if \quad 5s^{-1} < \dot{\varepsilon} < 200s^{-1} \end{cases} \tag{5}$$

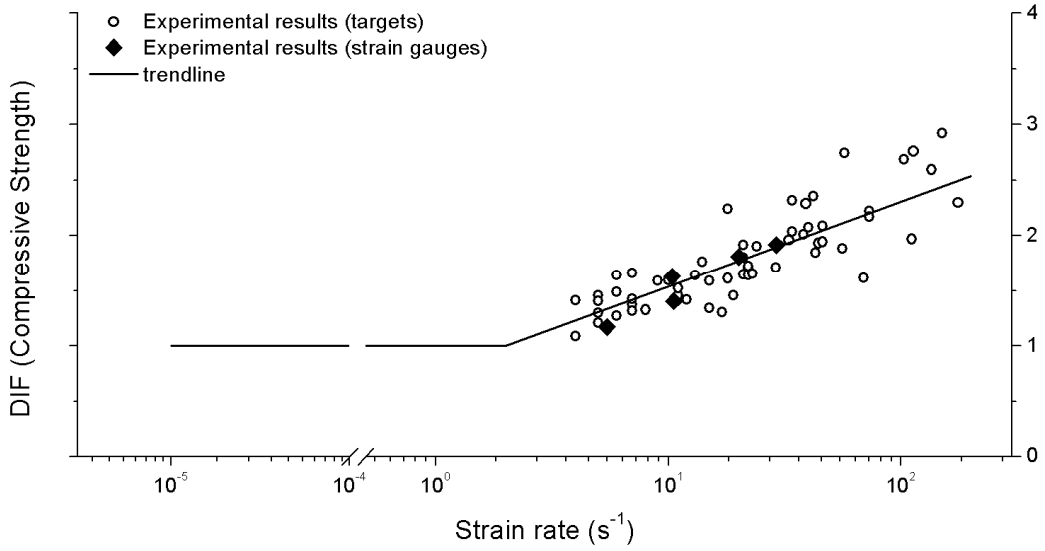

Figure 4: Example of DIF for compressive strength (for clay brick).

3 A Plastic Interface Model for High Strain Rates

In the present study, a rate dependent interface model is introduced to characterize the mortar behaviour, based in the original model of [12]. Depending upon the main failure mechanisms of masonry walls, the failure envelop is divided into three parts namely, tension cut-off, Coulomb friction, and elliptical cap, see Figure 5. Hence, each part has its own failure criterion presented in terms of k, where the k parameter is a scalar involved to measure the amount of softening and hardening in order to control the yield surface, and in terms of the stress vector σ. For a 3D configuration, $\sigma = \{\sigma, \tau_s, \tau_t\}^T$, $D = diag\{k_n, k_s, k_t\}$ and $\varepsilon = \{\Delta u_n, \Delta u_s, \Delta u_t\}^T$. The subscripts n, s, t denote the normal and two perpendicular shear components.

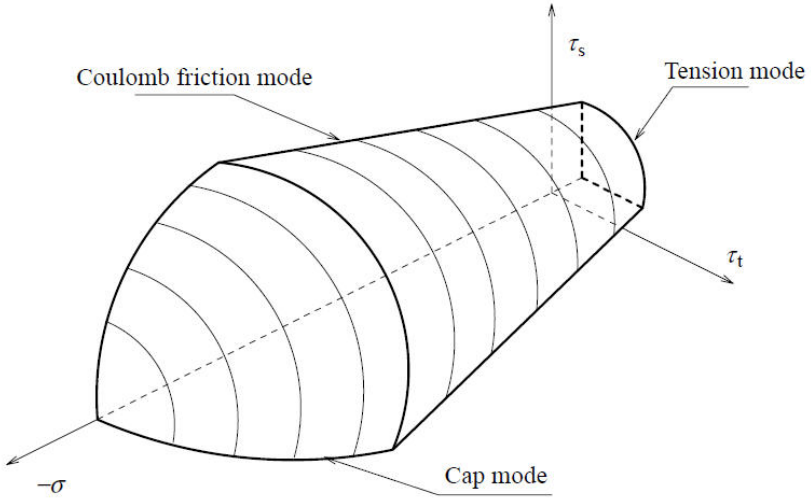

Figure 5: 3D Failure envelope of the interface cap mode.

In order to consider the high strain rate effects on the interface material model, dynamic increase factors (DIFs) are defined to control the failure envelop, as addressed above. These factors multiply the material parameters to expand or to contract the failure envelope at different strain rate levels. For the tension cut-off mode, the yield function is given as follows:

$$f_1\left(\sigma, k_1\right) = \sigma - \bar{\sigma}_1(k_1) \tag{6}$$

where the scalar σ denotes the normal stress and k_1 denotes a scalar to measure the amount of softening. For the hardening/softening behaviour the yield stress value varies exponentially as

$$\bar{\sigma}_1 = f_t \exp(-\frac{f_t}{G_f^I} k_1) \tag{7}$$

Here, f_t is the tensile strength of the joint (usually equal to the unit-mortar interface) and G_f^I is the mode I fracture energy. The DIFs are applied to the uniaxial tensile strength and the fracture energy to obtain

$$f_t = DIF \times f_{t_0} \tag{8}$$

$$G_f^I = DIF \times G_{f_0}^I \tag{9}$$

where, f_{t_0} and $G_{f_0}^I$ are the quasi-static strength and fracture energy under uniaxial tension, respectively. In case of strain hardening, the scalar $\dot{k}_1$ reads, in rate form,

$$\dot{k}_i = \sqrt{(\dot{\varepsilon}_i^{\,p})^T \, \dot{\varepsilon}_i^{\,p}} \tag{10}$$

where the plastic strain rate is given by $\dot{\varepsilon}_i^{\,p} = \dot{\lambda}_i \frac{\partial g_i}{\partial \sigma}$. Here, g_i is the plastic potential and $\dot{\lambda}_i$ is the plastic multiplier. As in mode I the normal plastic relative displacement governs the softening behaviour, $\dot{k}_1$ can be assumed equal to

$$\dot{k}_1 = \left|\Delta \dot{u}_n^p\right| = \dot{\lambda}_1 \tag{11}$$

When yielding occurs, the plastic corrector brings back the stress update to the yield surface by applying locally a Newton-Raphson method to solve the nonlinear system and updating the stress tensor and the user-defined state variables. In a plasticity model, it is worth to mention that at the starting point the stress is assumed to be elastic (considering a trial value), such as $\sigma_{n+1} = \sigma^{trial}$, $\dot{k}_{n+1} = 0$, and $\dot{\lambda}_{n+1} = 0$,

which is obtained by the elastic predictor. The unknowns of the nonlinear system of equations that arise in this update procedure are the stress components, $\dot{k}_{n+1}$ and $\dot{\lambda}_{n+1}$. The stress update equations are given for a finite step are given by

$$\sigma_{n+1} = \sigma^{trial} - D\dot{\varepsilon}^{p}_{n+1} \tag{12}$$

with $\sigma^{trial} = \sigma_n + D\dot{\varepsilon}^{e}_{n+1}$. The stress update equations can be easily obtained from the set of non-linear equations system

$$\begin{cases} \sigma_{n+1} = \sigma^{trial} - \dot{\lambda}_{1,n+1} k_n \\ \tau_{n+1} = \tau^{trial} \end{cases} \tag{13}$$

where $\tau = \sqrt{\tau_s^2 + \tau_t^2}$ is assumed for 3D configuration. The derivative with respect to $\Delta\lambda_{n+1}$ is needed for the iterative local Newton-Raphson method, given by

$$\left.\frac{\partial f_1}{\partial \dot{\lambda}_1}\right|_{n+1} = -k_n - \frac{\partial \bar{\sigma}_1}{\partial k_1} \tag{14}$$

In mode II, the Coulomb friction yield criterion reads

$$f_2(\sigma, k_2) = \tau + \sigma \tan\varphi(k_2) - \bar{\sigma}_2 \tag{15}$$

Here, τ and $\bar{\sigma}_2$ are given

$$\tau = \sqrt{\tau_s^2 + \tau_t^2} \tag{16}$$

$$\bar{\sigma}_2 = c \exp(-\frac{c}{G_f^{II}} k_2) \tag{17}$$

where, c denotes the cohesion of the unit-mortar interface, G_f^{II} is fracture energy in mode II, and ϕ denotes the friction angle.

The DIFs are applied to the cohesion, and mode II fracture energy and read

$$c = DIF \times c_0 \tag{18}$$

$$G_f^{II} = DIF \times G_{f_0}^{II} \tag{19}$$

Again, here, c_0 and $G_{f_0}^{II}$ are the quasi-static cohesion and fracture energy under shear, respectively. A non-associated plastic potential g_2 is defined as

$$g_2 = \tau + \sigma \tan\psi - c \tag{20}$$

Here, $\tan\psi$ is the dilatancy angle. In terms of pure shear, the shear plastic relative displacement can be assumed to control the softening behaviour as

$$\dot{k}_2 = \left|\Delta \dot{u}_s^p\right| = \dot{\lambda}_2 \tag{21}$$

Manipulating the stress update equations, it is possible to obtain

$$\begin{cases} \sigma_{n+1} = \sigma^{trial} - \dot{\lambda}_{2,n+1} k_n \tan\psi \\ \tau_{n+1} = \tau^{trial} - \dot{\lambda}_{2,n+1} k_s \dfrac{\tau^{trial}}{\left|\tau^{trial}\right|} \end{cases} \tag{22}$$

The derivative required for the iterative local Newton-Raphson method reads

$$\left.\frac{\partial f_2}{\partial \dot{\lambda}_2}\right|_{n+1} = -k_n \tan\phi \tan\psi - k_s - \frac{\partial \bar{\sigma}_2}{\partial k_2} \tag{23}$$

For the compressive cap mode, the yield function can be better provided in matrix notation form as

$$f_3(\sigma, k_3) = \frac{1}{2}\sigma^T P \sigma + p^T \sigma - (\bar{\sigma}_3(k_3))^2 \tag{24}$$

where P is the projection matrix, given by $diag\{2C_{nn}, 2C_{ss}\}$, and is the projection vector, given by $\{C_n, 0\}^T$. Here, C_{nn} and C_n are material parameters that determine the contribution of each stress component to failure, assumed equal to 1 and 0, respectively (this provides a centred ellipsoid in the origin). Parameter C_{ss} governs the intersection of the ellipsoid with the shear stress axis so that the maximum shear stress τ_u is given by $\tau_u = \dfrac{f_m}{\sqrt{C_{ss}}}$, where f_m denotes the masonry compressive strength, and a value of 9 is recommended [12].

The following law is used to introduce the hardening/softening behaviour of masonry under uniaxial compression:

$$\bar{\sigma}_a(k_3) = \bar{\sigma}_i + (\bar{\sigma}_p - \bar{\sigma}_i)\sqrt{\frac{2k_3}{k_p} - \frac{k_3^2}{k_p^2}} \tag{25}$$

$$\bar{\sigma}_b(k_3) = \bar{\sigma}_p + (\bar{\sigma}_m - \bar{\sigma}_p)\left(\frac{k_3 - k_p}{k_m - k_p}\right)^2 \tag{26}$$

$$\begin{aligned} &\bar{\sigma}_c(k_3) = \bar{\sigma}_r + (\bar{\sigma}_m - \bar{\sigma}_r)\exp\left(m\frac{k_3 - k_m}{\bar{\sigma}_m - \bar{\sigma}_r}\right) \\ &with \quad m = 2\frac{\bar{\sigma}_m - \bar{\sigma}_p}{k_m - k_p} \end{aligned} \tag{27}$$

Here, the subscripts *i*, *m*, *p* and *r* in the yield value and scalar *k* indicate the initial, medium, peak and residual values, respectively, providing parabolic hardening, followed by exponential softening [12].

The dynamic increase factors of uniaxial compressive strength and hardening are utilized to shift the failure envelop at different strain rates.

$$f_m = DIF \times f_{m_0} \tag{28}$$

$$k_m = DIF \times k_{m_0} \tag{29}$$

$$k_p = DIF \times k_{p_0} \tag{30}$$

Here, f_{m_0}, k_{p_0}, k_{m_0} and are quasi-static strength, amount of hardening corresponding to uniaxial compressive strength and scalars defining the inelastic law.

In order to illustrate the response of the developed material model in the prediction of joint behaviour and appropriate implementation of user-defined subroutine in ABAQUS, simple numerical models of a rigid block were developed and submitted under uniaxial tension, pure shear, and uniaxial compression at different strain rate levels. The response of the mode subjected to each type of loading is given in Figure 6. Typical material properties adopted for the joints and the dynamic increase factors are used here, see Table 1. Here, k_n and k_s are the normal and tangential interface stiffness.

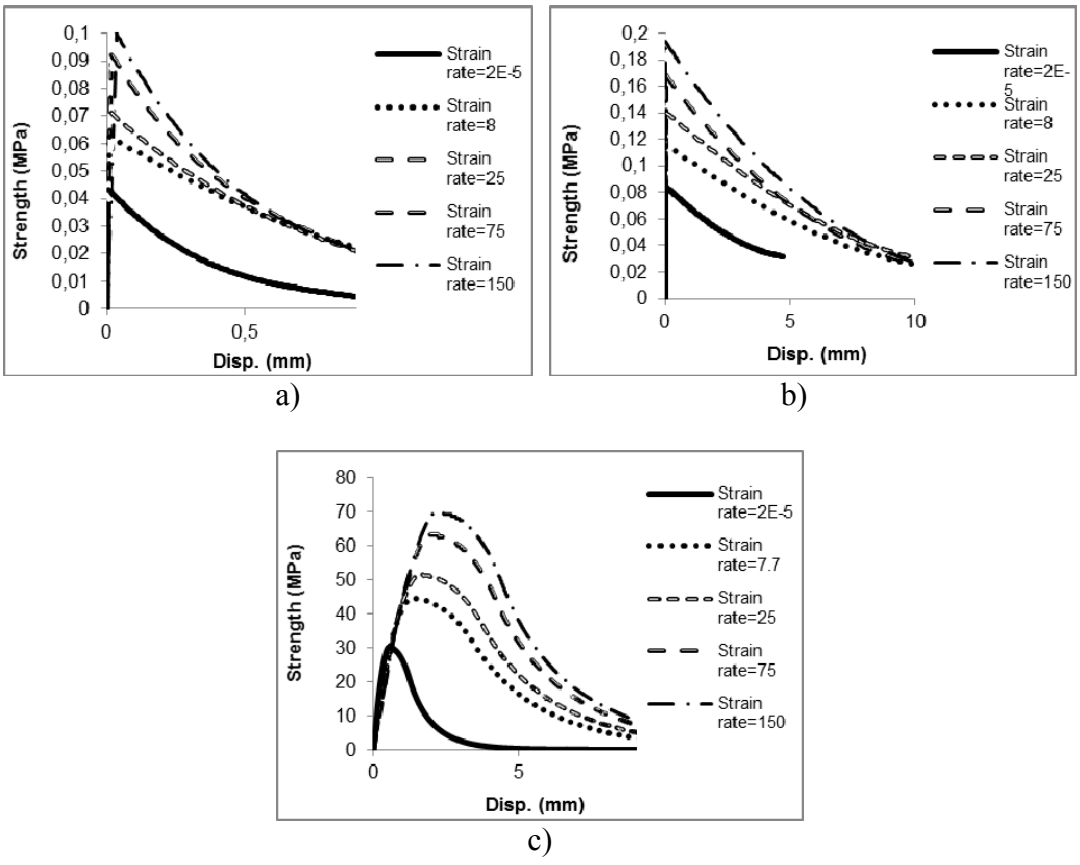

Figure 6: Uniaxial behaviour of the model under increasing strain rate: a) tension; b) shear; c) compression.

	Inelastic properties										Elastic properties	
	Tension		Shear				Cap					
	f_t (MPa)	G_{fI} (N/m)	c (MPa)	$\tan\phi$	$\tan\psi$	G_{fII} (N/m)	f_m (MPa)	C_{SS}	k_m (m)	k_p (m)	k_n (N/m^3)	k_s (N/m^3)
	0.043	17.2	0.083	0.5	0	400	30	9	1E-3	0.2E-3	9.26E10	5.447E10
Strain rate	DIF											
2E-5	1	1	1	-	-	1	1	-	1	1	1	1
8	1.48	2.96	1.48	-	-	2.96	1.48	-	2.96	2.96	0.71	0.71
25	1.71	3.14	1.71	-	-	3.14	1.71	-	3.14	3.14	0.69	0.69
75	2.1	3.31	2.1	-	-	3.31	2.1	-	3.31	3.31	0.66	0.66
150	2.33	3.4	2.33	-	-	3.4	2.33	-	3.4	3.4	0.65	0.65

Table 1: Material properties of joints and corresponding.

4 Validation with Out of Plane Masonry Walls

The experimental data in [8] is used for validation of the developed numerical model. In their study, 21 full-scale unreinforced walls, made of bricks and blocks bonded by mortar layers at bed and head joints, were subjected to low velocity impacts with different applied impulses applied by square steel plate placed at mid-length. Two walls, namely URP1 and URP2 are considered here. These walls have clear size of 5.75 x 1.13 x 0.20 m^3 and 9.15 x 1.13 x 0.22 m^3, respectively, using mortar bonded concrete block-work. Two stiff concrete blocks served as abutments and were constructed at the extremes of the walls. The impact load was applied through a steel plate at mid-height of the wall. In the numerical modelling, the applied load is modelled by a triangular load-time distribution with peak force of 90 KN and 110 KN reaches at 22.9 msec and 25 msec, respectively.

The dynamic interface model is attributed to 3D interface elements to take into account the joint behaviour during numerical simulation. Since the failure mechanisms of masonry walls subjected to high strain rate loads mostly deal with failure in joints, no serious damage is expected for the units and they were considered elastic and modelled by 3D solid elements. Typical tensile material properties are adopted for the joints.

A comparison between the predicted wall response and field test data is carried out using crack patterns and deflection, to evaluate the accuracy of the predictions. Figures 7 and 8 show the observed crack patterns and deformed shapes of the tested parapets, URP1 and URP2 subjected to out of plane impact loads.

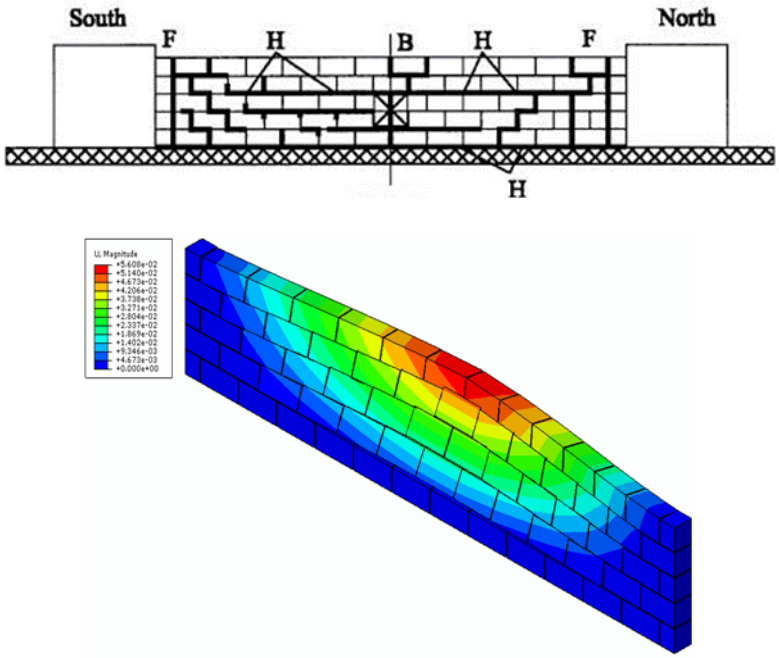

Figure 7: Wall URW1. Experimental (after the test) and numerical (for maximum displacement) observed behaviour.

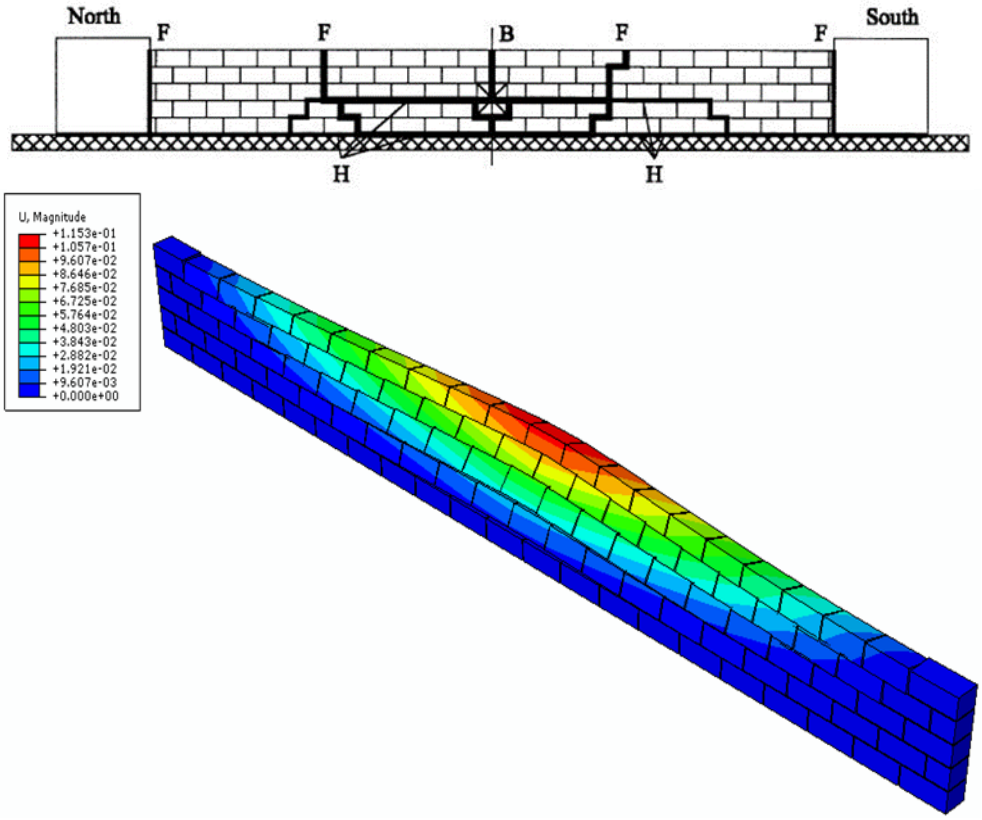

Figure 8: Wall URW2. Experimental (after the test) and numerical (for maximum displacement) observed behaviour.

According to simulations, it is noted that vertical cracks were formed over entire height of the parapet URP1 at the centre and to each side, and both right and left parts rotated inside. Moreover, the cracks are distributed along the length of the parapet, see Figure 7. For the wall URP2, besides a vertical fracture line occurred at the centre over the entire height of the wall, diagonal fractures, distributed around the centreline in both sides, were observed connected to horizontal cracks, see Figure 8. Some horizontal cracks are noticed in joints at lower levels. It is evident that increasing the length of the wall, reduces the effect of the boundaries and cracks localize close to the impact zone. An appropriate agreement in prediction of failure modes is apparent between the tests and simulations.

Next, a comparison is made for the displacement vs. time response of the walls. The displacements are recorded at the points located at mid-height and 580 mm above the base, offset by 500 mm and 250 mm to the left of the centreline, respectively. As shown in Figure 9, the numerical models can predict the high strain rate response of the walls including magnitude of peak displacement and post-peak trend close to the observed test results. Here it is noted that for wall URP1 there is a pronounced built up of stiffness found in response due to the inertial forces and acceleration of movement. For the wall URP2, The numerical response is shifted to the origin because the experiment does not show the initial acceleration of movement.

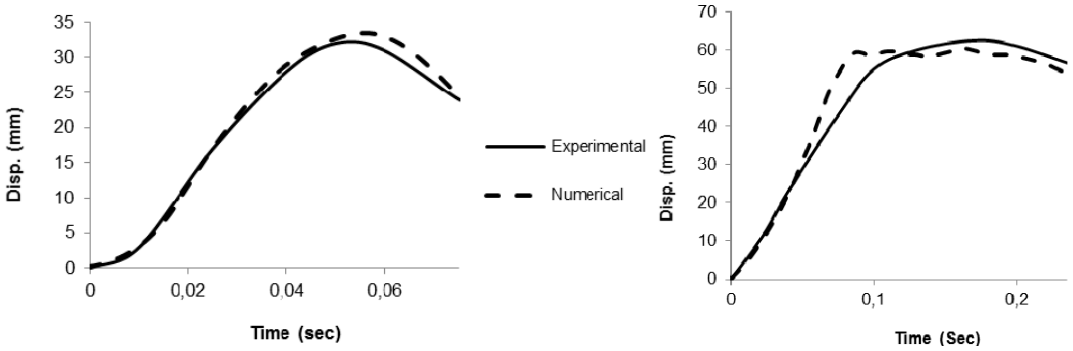

Figure 9: Displacement vs. time response of the wall URP1 (left) and URP2 (right).

5 Conclusions

Understanding the strain rate effect on masonry materials is important for proper modelling and design of masonry structures under high velocity impacts or blast loads. A large experimental campaign was performed on different loading regimes and different materials. Masonry specimens and its components, clay brick and mortar, were tested under quasi-static regime – strain rate of 10^{-5} s^{-1} – and dynamic regime with strain rates ranging from 2 s^{-1} up to 200 s^{-1}. It was found that the mechanical properties of these materials increase with the increase in strain rate, having DIFs ranging from 2 to 6 for a strain rate of 200 s^{-1}.

Next, a rate dependent dynamic interface model to for the numerical simulation of masonry structures using a micro-modelling approach is presented. The 3D interface model is implemented as a user-defined subroutine in the finite element code ABAQUS. The adequacy of the material model to replicate measured dynamic increase factors measures experimentally is demonstrated by applying various uniaxial loading conditions. A comparison between numerical predictions and field test data of two full scale masonry walls is carried out, including displacement-time response diagrams and failure mechanisms. It can be inferred from the numerical results that the model can predict the maximum deflection and failure mode over the entire length of the walls, with good agreement.

References

[1] M.A. Meyers, *Dynamic behaviour of material*, J John Wiley & Sons Publications, USA, 1994.

[2] J. Baylot, B. Bullock, T. Slawson, S., Woodson, "Blast response of lightly attached concrete masonry unit walls", Journal of Structural Engineering, 131(8), 1186-1193, 2005.

[3] H. Hao, B.G. Tarasov, "Experimental study of dynamic material properties of clay brick and mortar at different strain rates", Australian Journal of Structural Engineering, 8(2), 117-132, 2008.

[4] S. Burnett, M. Gilbert, T. Molyneaux, A. Tyas, B. Hobbs, G. Beattie, "The response of masonry joints to dynamic tensile loading", Materials and Structures, 40(1), 517-527, 2007.

[5] D. Asprone, E. Cadoni, A. Prota, G. Manfredi, Dynamic behaviour of a Mediterranean natural stone under tensile loading, "International Journal of Rock Mechanics and Mining Sciences", 46(3), 514-520, 2009.
[6] R. Varma, C. Tomar, S. Parkash, V. Sethi V, "Damage to Brick Masonry Panel Walls Under High Explosive Detonations", ASME-PUBLICATIONS-PVP 351, 207-216, 1996.
[7] J.T. Baylot, B. Bullock, T.R. Slawson, S.C. Woodson, "Blast response of lightly attached concrete masonry unit walls", Journal of Structural Engineering, 131(8), 1186-1193, 2005.
[8] M. Gilbert, B. Hobbs, T. Molyneaux, "The performance of unreinforced masonry walls subjected to low-velocity impacts: experiments. International" Journal of Impact Engineering, 27(3), 231-251, 2002.
[9] P.B. Lourenço, "Computations of historical masonry constructions", Progress in Structural Engineering and Materials, 4(3), 301-319, 2002.
[10] P.B. Lourenço, G. Milani, A. Tralli, A. Zucchini, "Analysis of masonry structures: review of and recent trends of homogenisation techniques", Canadian Journal of Civil Engineering, 34 (11), 1443-1457, 2007.
[11] Pereira, J.M., *Security Evaluation and Design of Structures Subjected to Blast Loading*, PhD Thesis, University of Minho, 2014.
[12] P.B. Lourenço, J.G. Rots, Multisurface interface model for the analysis of masonry structures, Journal of Engineering Mechanics, ASCE, 123(7), 660-668, 1997.